Distribution Agreement

In presenting this thesis as a partial fulfillment of the requirements for a degree from Emory University, I hereby grant to Emory University and its agents the non-exclusive license to archive, make accessible, and display my thesis in whole or in part in all forms of media, now or hereafter now, including display on the World Wide Web. I understand that I may select some access restrictions as part of the online submission of this thesis. I retain all ownership rights to the copyright of the thesis. I also retain the right to use in future works (such as articles or books) all or part of this thesis.

Anirudh Raghavan April 8, 2022

In Vitro Conditions for Assembly of the Respiratory Syncytial Virus Nucleocapsid into Ring-like Oligomers or Helical Filaments

by

Anirudh Raghavan

Dr. Bo Liang

Adviser

Department of Biology

Dr. Bo Liang

Adviser

Dr. Anita Corbett

Committee Member

Dr. Frank McDonald

Committee Member

2022

In Vitro Conditions for Assembly of the Respiratory Syncytial Virus Nucleocapsid into Ring-like Oligomers or Helical Filaments

By

Anirudh Raghavan

Dr. Bo Liang

Adviser

An abstract of
a thesis submitted to the Faculty of Emory College of Arts and Sciences
of Emory University in partial fulfillment
of the requirements of the degree of
Bachelor of Science with Honors

Department of Biology

2022

Abstract

In Vitro Conditions for Assembly of the Respiratory Syncytial Virus Nucleocapsid into Ring-like Oligomers or Helical Filaments

By Anirudh Raghavan

A hallmark of the genomes of non-segmented negative-sense (-) RNA viruses is that the genomic RNA never exists in an isolated configuration – it is instead encapsidated by the nucleoprotein (N) into highly structured and ordered helical nucleocapsids (NCs), reminiscent of nucleosomes in eukaryotic cells. The NCs of the respiratory syncytial virus (RSV) can display multiple morphologies, including spherical, asymmetric, and filamentous conformations. Here, we analyze the morphology of recombinant nucleocapsid-like particles (NCLPs) of the respiratory syncytial virus assembled under different conditions. We examined the effects of modifying the integrated RNA length, and the effects of variations in buffer conditions, including salt concentration, ionic strength, pH, and the presence of reducing reagents under cryogenic conditions to assemble N into ring-like oligomers or higher-order helical filaments. We confirmed the conformational variability of the reconstituted RSV NCLPs and the constraints of the nucleocapsids upon binding to RNA using negative-stain and cryo-EM imaging. Our findings provide insights into N and RNA complexation into a loose oligomer form versus a tight helical skeleton form. We postulate that RNA length as well as flexibility of the C-terminal domain (CTD) arm of each N protomer, which can be manipulated *in vitro* via varying buffer conditions, affect RNA-binding as well as N oligomerization into higher-order structures. We hope that elucidation of NC assembly morphologies and identifying possible mechanisms leading to the formation of each can aid in future structural studies as well as help to develop future interventions to hinder efficient NC assembly, an essential prerequisite for RSV infection and proliferation.

In Vitro Conditions for Assembly of the Respiratory Syncytial Virus Nucleocapsid into Ring-like Oligomers or Helical Filaments

By

Anirudh Raghavan

Dr. Bo Liang

Adviser

A thesis submitted to the Faculty of Emory College of Arts and Sciences
of Emory University in partial fulfillment
of the requirements of the degree of
Bachelor of Science with Honors

Department of Biology

2022

Acknowledgements

I would like to personally thank Dr. Bo Liang, my project advisor, for providing valuable and continued support and guidance throughout the design, experimental phase, and write-up phases of the project. I would like to express my gratitude to my post-doctoral mentor Dr. Yunrong Gao, for aiding with cryo-EM imaging and structural modeling on this project.

I would also like to thank my committee members, Dr. Frank McDonald & Dr. Anita Corbett, for serving on my honors committee, providing academic mentorship, and being greatly inspirational professors.

Table of Contents

Introduction

Respiratory Syncytial Virus (RSV) is a significant viral pathogen most commonly responsible for inducing lower respiratory tract diseases in infants, the elderly, and immunocompromised individuals globally [1]. In infants, RSV primarily induces bronchiolitis and pneumonia [2], and pathology manifests more generally as immunological hypersensitivity in the respiratory tract that has been associated with increased vulnerability to the development of allergy and asthma [3,4]. RSV is classified as an enveloped non-segmented negative-strand (NNS) RNA virus of the *Paramyxoviridae* family, more specifically categorized into the *Pneumovirus* genus of the *Pneumoviridae* subfamily [5].

The genome of the RSV A2 strain is comprised of 15,222 nucleotides and contains ten sequential genes which encode 11 different proteins (nine structural and two non-structural) (Fig. 1). In the 3' to 5' order, these are the genes encoding non-structural proteins 1 and 2 (NS1 and NS2), the nucleoprotein (N), the phosphoprotein (P), the matrix protein (M), the small hydrophobic protein (SH), the glycoprotein (G), the fusion protein (F), M2-1 and M2-2, and a large protein (L, an RNA-dependent RNA polymerase) [6]. Each of these genes is situated between gene start (GS) and gene end (GE) sequences. The RSV genome also contains two extragenic regions: a 44-nucleotide leader (Le) sequence and a 155-nucleotide trailer (Tr) sequence at the 3' and 5' ends respectively that function as promoters for transcription [7].

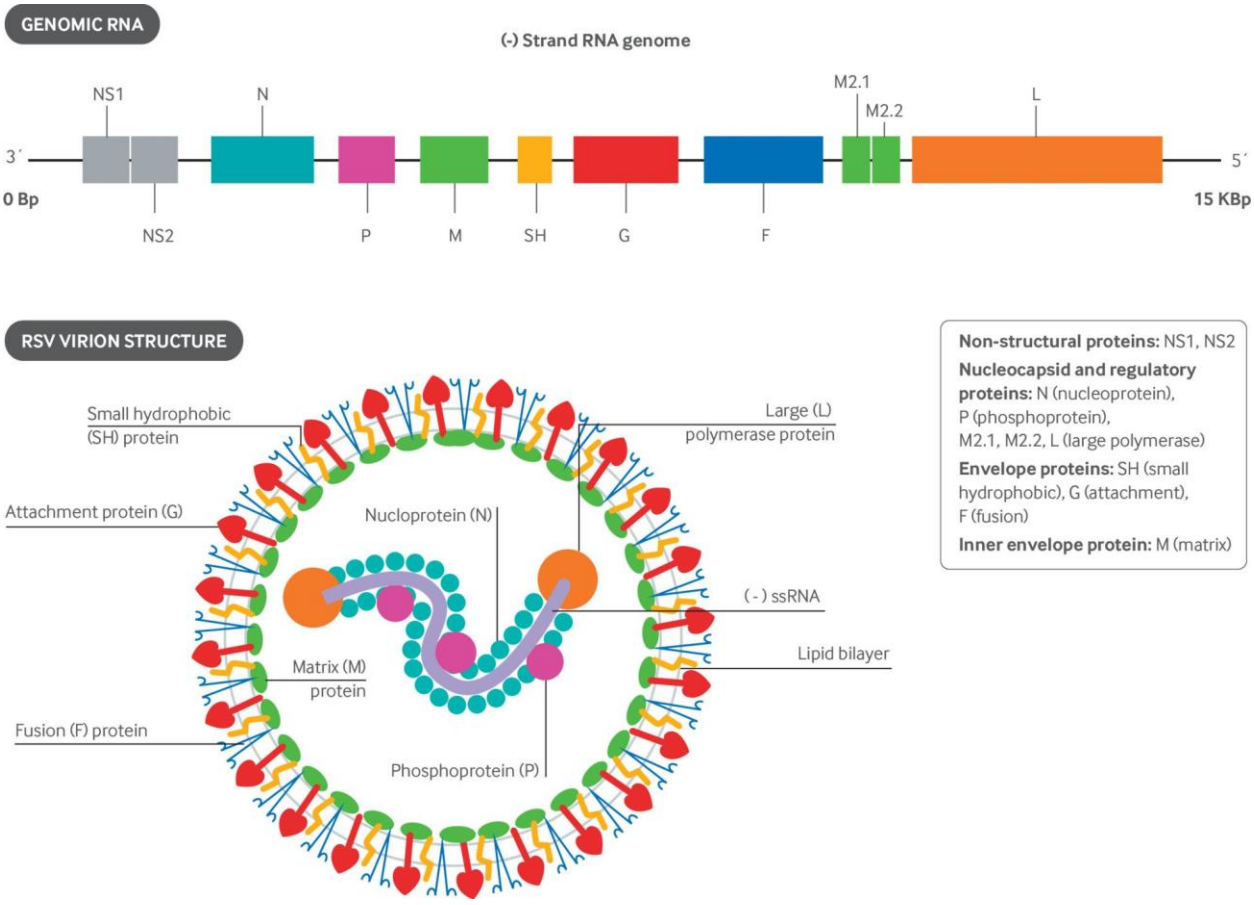

Figure 1: Structure of the Respiratory Syncytial Virus (RSV). Figure adapted from Nam, H. H., & Ison, M. G. (2019) [8].

The N protein has a mass of ~43 kDa and consists of 391 residues [9,10]. The RSV genomic RNA complexes with the N protein to form a helical ribonucleoprotein (RNP) complex, which is then used as a template for RNA synthesis and genome replication by the viral polymerase machinery [11]. N has been implicated in the impairment of T-cell activation as well as interference in the immune synapse between host antigen-presenting cells and T cells during viral infection [12]. Therefore, N has been characterized as a crucial virulence factor that debilitates acquired immunity, thereby increasing host susceptibility to RSV reinfection. P protein can interact with RNA-free N protein (N0) at the N protein N-terminal domain as well as with the N-RNA helical complex at the N protein C-terminal domain [13,14]. P can function as a chaperone to block coordination of the newly synthesized naked N protein with cellular RNA and/or

other N subunits. P functions both as a co-factor for RSV L-polymerase and as an inhibitor of self-aggregation of N, thereby affecting the efficiency of nucleocapsid assembly, modulating the activity of the RNA-dependent RNA polymerase, and thus affecting RNA synthesis [15,16].

The helical RNP of RSV has been previously characterized as a flexible left-handed helical structure with a pitch of 68 Å [17] (Fig. 2). Each N subunit of the helical nucleocapsid (NC) coordinates with seven ribonucleotides and is assembled as a core region, with a distinct N-terminal domain (NTD) and C-terminal domain (CTD) each having their own extensions, termed the N-arm and the C-arm (Fig. 3) [11]. The N-arm and C-arm serve as linkers between subunits in the RNA-bound ring by forming stabilizing interactions with adjacent subunits in the N-RNA complex at the 5' and 3' ends, respectively [11]. The RNA is then tethered to a groove formed at the interface between the N- and C-terminal domains. Further, we have previously reported that functionally the N-arm assists in oligomerization of N-RNA by inserting into the compact fold of the adjacent N subunit in the RNA-bound ring, while the C-arm blocks accessibility to cellular RNA when N protein is expressed [18].

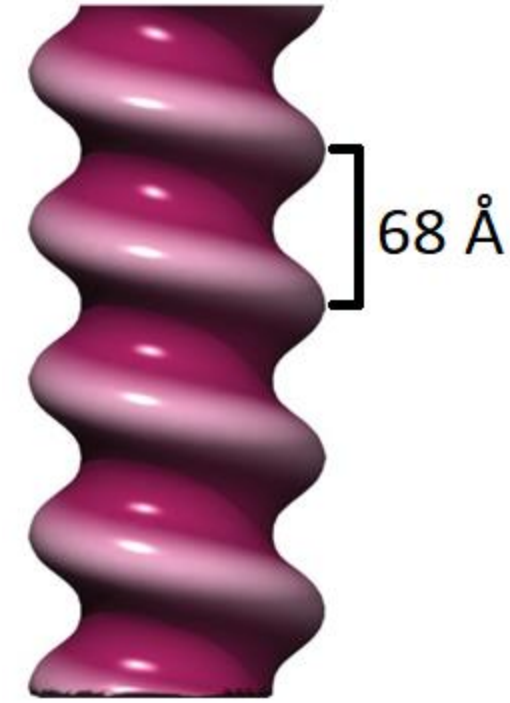

Figure 2: The ribonucleoprotein (RNP) complex of RSV is a left-handed helix with a pitch of 68 Å.

Figure adapted from Bakker, S. E., et al. (2013) [17].

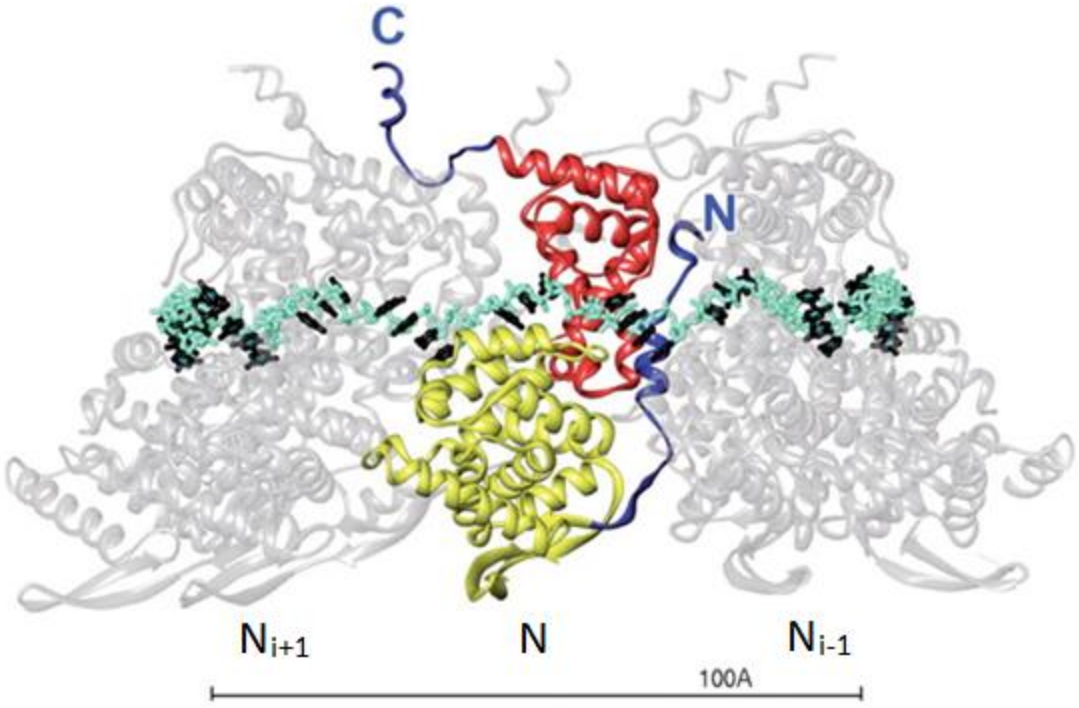

Figure 3: In a single turn of the RNP complex of RSV, each nucleoprotein (N) subunit of the RNP coordinates with seven ribonucleotides. The N-terminal domain (NTD) & C-terminal domain (CTD) are depicted with their respective extensions - N-arm and the C-arm. The NTD-arm packs against the flank of the previous protomer (the NTD-arm of N_{i+1} packs against N_i). The CTD-arm in turn latches onto the top of the CTD of the next protomer (the CTD-arm of N_i latches onto the CTD of N_{i+1}). The RNA (shown in turquoise and black) is tethered to a groove formed at the interface between the N- and C-terminal domains. Figure adapted from Tawar, R. G., et al. (2009) [11].

Despite successful reconstitution of the RSV polymerase transcription assay in vitro, reconstructing the N–RNA template into helical filaments presents a significant challenge as N protein can bind non-specifically to random cellular RNA, rather than RSV-specific viral RNA, to form nucleocapsid-like particles (NCLPs) upon recombinant expression of N [11,17]. We have previously demonstrated that the N-terminal domain of P protein, P_{NTD}, can be exploited as a chaperone to block N association with non-specific viral RNAs via co-expression of P_{NTD} and N, successfully obtaining RNA-free N-P complex in RSV on a large scale in a trackable manner [18]. We also previously discovered that efficient NCLP assembly in RSV with purified RNA-free N is dependent on the length and specific sequence of the RNA and can result in varied NC morphologies [18]. However, as observed in Vesicular Stomatitis Virus (VSV), a member of the *Rhabdoviridae* family of viruses, *in vitro* assembly of purified nucleocapsids can show morphological variation with notable conformational flexibility when simply constructed in buffers with varying pH and ionic strength conditions [19]. The variation was identified via negative-stain and cryo-EM analysis, which showed marked differences in the pitch and coiling of helical N-RNA trunks as well as the tightness of coiling of the conical tip (Fig. 4). These two structural features together generate the representative bullet-shaped VSV nucleocapsid conformation [19].

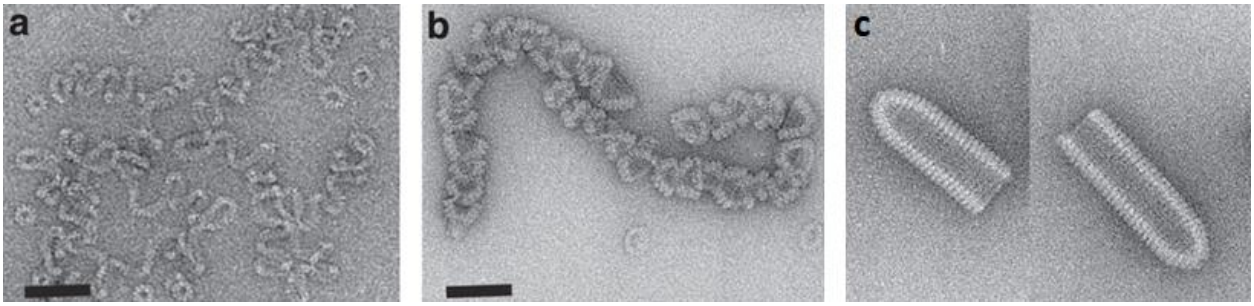

Figure 4: In vitro assembly of purified nucleocapsids of Vesicular Stomatitis Virus (VSV) showed morphological variation with conformational flexibility when assembled in buffers with varying pH and ionic strength conditions.

Negative stain images shown are of three different morphologies that were noted due to conformational flexibility of the nucleocapsid: (a) Loosely coiled N-RNA ribbons (negative stain). (b) Strings of tips (negative stain), and (c) N-RNA bullets. Figure adapted from Desfosses, A., et al. (2013) [19].

In this study, we aimed to successfully reconstitute RNA-free nucleoprotein (N) with P for proper N-RNA construction in vitro with polyA7/Tr70 RNA sequences so that NC morphologies in vitro can be qualitatively distinguished between using cryo-EM and negative-stain EM imaging. We further aim to visualize N-RNA association via gel electrophoresis shift assays and propose speculative models of mechanisms that we think may be involved and are manipulated by changes in buffer conditions. We demonstrate that morphological selection occurs between RSV rigid N-RNA ring formation, aggregation of incomplete ring assemblies, and flexible continuous higher order helical oligomeric structures. This selection was observed to be dependent upon the length of RNA as well as buffer salt concentration, ionic strength, pH, and inclusion of DTT using electron microscopy (negative-stain imaging and cryo-EM). We hypothesize that the aforementioned conditions primarily influence the flexibility of the RSV N CTD-arm and thus alter its consequent stabilizing attachment points to shift the equilibrium towards a specific structure. We hope this can further shed light on RSV NC conformations *in vitro* and help develop future interventions to hinder efficient NC assembly, an essential prerequisite for RSV infection and proliferation.

Materials & Methods

Cloning, expression, and purification of the N^0-P_{NTD}, in-vitro construction of the N-RNA complex, as well as negative-stain and cryo-EM sample preparation and imaging, were performed as described [18,20].

N^0-P_{NTD} Plasmid Cloning

Full-length RSV N, consisting of residues 1-391, was fused with a His_{10}-tobacco etch virus cleavable tag at the N-terminus and subsequently cloned in tandem with the N-terminal domain of RSV P, consisting of residues 1-126, into a polycistronic plasmid. The final His_{10}–tobacco etch virus–NP_{NTD} was constituted via independently amplifying genes encoding RSV N and P with a region of overlap covering the 3' end of N

and 5’ end of P, followed by fusion via PCR amplification. A brief schematic depicting the plasmid section utilized is shown in Fig. S1.

N^0-P_{NTD} Protein Expression & Purification

The *E. coli* BL21(DE3) chemically competent strain was utilized for producing N^0-P_{NTD}. Cells were cultured at 37°C in Miller’s Luria Broth medium until A_{600} reached 0.8. Expression was induced after lowering temperature to 16 °C and incubating with 0.5 mM isopropyl 1-thio-β-D-galactopyranoside overnight. Cell lysis was conducted by sonication in lysis buffer A (50 mM sodium phosphate at pH 7.4, 500 mM NaCl, 5 mM imidazole, 10% glycerol, and 0.2% NP-40 detergent) and subsequent centrifugation. The supernatant was then loaded onto a cobalt column equilibrated with lysis buffer. The cobalt column was washed with buffer B (50mM Tris-HCl at pH 7.4, 1 M NaCl, 10% glycerol, and 5 mM imidazole) and buffer C (50 mM Tris-HCl at pH 7.4, 500 mM NaCl, 10% glycerol, and 5 mM imidazole). The protein was eluted from the cobalt column with buffer D (50 mM Tris-HCl at pH 7.4, 500 mM NaCl, and 400 mM imidazole). Further protein purification was performed via Q column followed by isolation using a Superdex 200 gel-filtration column equilibrated with buffer E (20 mM HEPES at pH 7.4 and 200 mM NaCl).

Electrophoretic Mobility Shift Assay (EMSA) for detecting N^0-P_{NTD}-RNA interactions

Purified stock full-length-N-$P_{1\text{-}126}$-His utilized in this assay was at a concentration of 5.7 mg/mL. The RNA transcript utilized was based on a truncation of the RSV CAT minigenome (Fig. S2), specifically the Le39 sequence followed by a poly7A sequence. The RNA concentration was 1 µM. The buffer used for subseqent serial dilution of purified stock protein was comprised of 50 mM Tris pH 8.0, 250 mM NaCl, 10% glycerol, and no imidazole (dilution buffer). A dilution schematic is displayed in Fig. S3. 3 µL 50% glycerol was added to each sample, and 1 µL of the 1 µM RNA (46nt) sample was added to all tubes excluding the protein-only control, and the samples were incubated overnight at 4°C. 3 µL loading dye

was added prior to loading onto a 5% Tris-Glycine Gel. The gel was pre-run for 20 minutes prior to sample loading into wells. The gel was run at 120 V and 400 mA for 60 minutes in an ice-water bath, and was subsequently stained for RNA detection with 5 µL Ethidium Bromide added to 50 mL of dilution buffer. RNA staining was done for about 25 minutes prior to imaging, and was subsequently stained for protein presence with Coomassie Blue with gentle shaking overnight. The gel was then destained for about 2 hours with a destaining buffer consisting of water, methanol, and acetic acid in a ratio of 50/40/10 (v/v/v) prior to scanning. There is evidence of binding interactions between RSV N^0P and RNA 46nt (Le39 + poly7A), and this is shown in Fig. S5.

In-vitro construction of N-RNA complex

Purified N_0–P_{NTD} and RNA oligos, purchased as 0.1M or 1M stock from Integrated DNA Technologies, were co-incubated with a molar ratio of 1:1.5 in buffer E for 1 hour at room temperature. The resulting complex was purified by gel filtration using a Superdex 200 Increase 10/300 GL column (GE Healthcare) equilibrated with buffer E. The N_0–P_{NTD} (mass: 58 kDa) was then stored as stock at a concentration of between 40-60 mg/ml. The RNA oligos used in this study were polyA7 (5-AAAAAAA) and Tr70 (5-ACGAGAAAAAAGUGUCAAAAACUAAUAUCUCGUAAUUUAGUUAAUACACAUAUAAACCAAUUAGAUUAGG).

Negative Stain EM Image Collection

4 µL of N-RNA sample was applied onto a fresh glow-discharged grid (Ted Pella 400-mesh copper grids with continuous carbon film). The sample was then blotted to a thin film using filter paper and subsequently stained with 1% w/v uranyl formate. EM was conducted using an FEI Talos L120C electron microscope operating at 120 keV and supplemented with an FEI Ceta 4k x 4k CMOS camera accessory. Sample micrographs were collected at magnifications of x73,000 (1.97 Å/pixel). The images were acquired at a defocus value of between -1.2 and -2.0 µm and an electron dose rate of about 25 $e^-/Å^2$.

Cryo-EM Sample Preparation and Image Collection

A total of 3.0 µl of the purified N-RNA complex at specified concentrations (assembly with poly7A: 0.27 mg/ml and 1.47 mg/ml; assembly with Tr70: 0.27 mg/ml, 0.30 mg/ml, 0.43 mg/ml, 0.6 mg/ml, 1.47 mg/ml) were applied to freshly glow-discharged Quantifoil R1.2/1.3 Micromachined Holey Carbon Grids. Grids were blotted for 3 seconds at ~90% humidity at room temperature and plunge-frozen in liquid ethane using the Cryoplunge 3 (Cp3) semi-automated plunge freezing instrument (Gatan Inc.). EM was performed using a Talos Arctica TEM operating at 200 kV with BioQuantum/K2 direct electron detector (Thermo Fisher) at Emory University. Sample micrographs were collected at magnifications of ×130,000 (1.045 Å/pixel). Movies were acquired at a defocus range between −1.25 and −2.5 µm with an electron dose rate was set to 1.365 e-/Å^2. The total exposure time of each movie was 10 seconds, resulting in a total accumulated dose of 55 e−/Å^2 fractionated into 40 frames (250 ms per frame for a total of 10 seconds).

Results

In this study, we describe the effects of *in vitro* manipulation of solution ionic strength, pH, inclusion of DTT, and usage of short polyadenylated RNA sequences on the propensity and efficiency of formation of RSV N-RNA nucleocapsid-like particles (NCLPs). From this point forward, we define propensity as the degree to which ring morphology is observable regardless of final morphology, and we define efficiency as the degree to which the ring morphology resembles a rigid-ring or a higher-order helical filament. We generally observe a level of NCLP assembly under all tested conditions, with the precondition that the integrity of N and RSV-specific RNA structures are maintained. This result validates the idea that polymerization of RSV N and RSV-specific RNA into a ring-like structure is a natural and favored association. NCLPs were assembled by incubating RNA-free N (N^0) with a fixed molar ratio of RNA

followed by isolation of N-RNA complexes via gel filtration chromatography. Cryo-EM imaging was then used to analyze NCLP ring assembly.

To maximize RSV NCLP particle coverage in the hole region of the Quantifoil grids for proper imaging, various strategies can be employed such as simply increasing particle concentration, usage of a mild detergent that preserves protein-protein & protein-RNA interactions, or the usage of thin-layer support films such as graphene or graphene oxide to which particles readily absorb [21]. Here, simply increasing the concentration of the RSV N-RNA complex led to observably greater particle coverage in the hole region. Observing RSV-specific N-Tr70 complex assembly in the absence of DTT resulted in perceivable aggregation across all concentrations used, suggesting that DTT assists in preventing aggregation and improving particle dispersion; a higher local concentration of N-RNA particles were indeed captured within the central hole region when increasing N-RNA construct concentration in solution without DTT (Fig. 5), though the resultant particles did not display perfect construction character and aggregation was consistently observed.

Reducing pH is a more controllable parameter than modifying salt concentration for finetuning efficient RSV N-RNA NCLP formation

RSV N-RNA assembly depends on both pH and ionic strength of solution. Increasing the ionic strength of the solution, by doubling the concentration of NaCl from 150 mM to 300 mM while keeping the pH of the solution static at pH 7.5, leads to less oligomeric aggregation and significantly greater rigid N-RNA ring formation propensity; however, under these conditions there is an increase in the level of incompletely formed rings (Fig. 6A, Fig. 6B). Similarly, we observe that increasing the ionic strength of the solution to a lesser extent by increasing NaCl concentration from 150 mM to 200 mM but reducing the pH from 7.5 to 5.0 leads to significantly greater N-RNA ring formation efficiency with relatively moderate assembly propensity; seemingly, a moderate reduction of pH and a slight increase in ionic

strength (Fig. 6C) leads to the highest efficiency of N-RNA ring assembly observed of the three conditions tested, but this did not necessarily translate to the highest propensity for assembly.

In the RSV N-RNA ring structure, the RNA is wound around the N-protein polymeric ring and is inserted into a cleft lined with positively charged/protonated residues which lies between the N-terminal domain (NTD) and C-terminal domain (CTD) of N. Previously, RNA-free N (N^0) and RNA-bound N-RNA in *Pneumovirus* have been characterized to differ in the alignment of the CTD-arm: the CTD-arm is oriented away from N in the RNA-bound state, subsequently clasping onto the next nucleoprotein protomer, but in the monomeric RNA-free N^0 form the CTD-arm links itself adjacent to the nucleoprotein core via stabilizing salt-bridge interactions [22]. Furthermore, when the CTD-arm is positioned against the core of N, the CTD-arm directly prevents RNA binding as the CTD-arm electrostatically interacts with and occupies the positively charged RNA binding cleft as in *Paramyxoviridae*, the stretch of residues in the CTD-arm with helical propensity consists of topologically conserved negatively charged residues (Fig. 10, Fig. 11) [16].

At higher ionic strengths, the stabilizing salt-bridges which shift the equilibrium towards the N^0 conformation can be masked, and this burial of salt bridging interactions can produce a destabilizing effect [23]. In the RNA-bound conformation of N, suppression of electrostatic interactions due to the higher ionic strength favors the concomitant positioning of (i) RNA nucleotides in the RNA-binding cleft and (ii) CTD-arm linkage with the next N protomer. One potential hypothesis for the perceived inefficiency of N-RNA ring construction despite the greatly increased propensity of N-RNA ring assembly in conditions of higher ionic strength (Fig. 6B) may involve excessive CTD-arm flexibility due to disruption of salt bridges which pack the CTD-arm against the core of N. In this vein, the high salt concentration/ionic strength of the solution may confer flexibility to the CTD-arm to the extent that it may be entropically disfavored to limit its flexibility, either via linkage to the consequent nucleoprotein protomer to form N-RNA oligomers or via association near the RNA binding groove of its resident N

protomer, even with the additional stability gain from the aforementioned interactions. The consequent effect of high ionic strength would be to shift the equilibrium to NCLP aggregation due to the large mismatch between propensity and efficiency of particle assembly.

Lowering the pH of the polymerization solution to 5.0 and slightly raising ionic strength via increasing the concentration of NaCl to 200 mM (Fig. 6C) results in greater efficiency of N-RNA ring assembly with a slightly attenuated propensity for polymerization relative to Fig. 6B. This also suggests that the increase in proton concentration by lowering the pH increases the ionic strength of the solution and confers the effects mentioned earlier, although the reduction of pH by 2.5 units does not seem to confer the same propensity for N-RNA ring construction as does directly increasing NaCl concentration in solution. We hypothesize then that altering pH is a more controllable intervention than altering NaCl concentration in solution directly for optimizing both propensity and efficiency of RSV N-RNA polymerization, and that we would expect N-RNA particle aggregation to increase with larger decreases in pH proportionally.

DTT preserves high RSV N:RNA NCLP formation efficiency in an RNA-length dependent manner & provides protection of RNA under high pH conditions

When examining RSV N-RNA assembly in the presence of dithiothreitol (DTT), a small-molecule redox agent which reduces disulfide bonds *in vitro*, we detected an increase in N-RNA ring formation propensity and efficiency relative to N-RNA ring assembly in the absence of DTT. DTT is a reducing agent which functions to mimic the cellular cytoplasmic reducing milieu – since this naturally resembles the ideal environment for NC formation, we predict that NC assembly in the presence of DTT will be optimal in propensity and construction efficiency. Previously it has been shown that key disulfide interactions for RSV infection are present in a region known as the cystine noose embedded in the glycoprotein (G-protein), which has been theorized to assist in viral attachment to human airway epithelial (HAE) cells via interaction with CX3C chemokine receptor 1 (CX3CR1) [24]. The ectodomain of G consists of four

cysteine residues bonded with two disulfide linkages, between positions 173 & 186 and between positions 176 and 182 respectively [25]. The cystine noose motif within this domain is composed of the residues between the cysteine residues at positions 182 and 186 and forms a CX3C motif (CXXXC) which interacts with CX3CR1 during infection [26,27]. Interestingly, however, past results depict that this conserved region is generally not essential for RSV replication, wherein it had been shown that removal of the CX3C motif and a flanking 13-amino acid sequence from RSV G exerted a negligible effect on infectivity and viral replication *in vitro*, and intracellular synthesis of G was also shown to be unaffected [28,29]. In analyzing a truncated construct of RSV-specific RNA (Tr70) and its association with N in the presence of DTT (Fig. 7B), relative to Fig. 6B we observed less ring aggregation and a larger proportion of complete NCLP formation, as well as a greater propensity for ring formation from the greater number of rings observed within the hole region of the EM grid. Our results suggest that DTT may confer increased CTD-flexibility of RSV N allowing for increased propensity for ring formation, with the length and nature of viral RNA dictating the ultimate completeness of the NCLP assembly. Conversely, DTT may exert a protective effect onto RNA in a length-dependent manner, as seen in the additional improvement in NCLP formation efficiency and reduction in incomplete NCLP aggregation assembly of Tr70 with RSV N in the presence of DTT within a higher pH buffer (Fig. 7C). Interestingly, extending on this, we find that the ideal pH condition for assembly of RSV N-Tr70 particles was markedly higher than shorter adenine-repeat RNA oligo constructs with RSV N, further reinforcing that DTT may most likely exert a protective effect on RNA, perhaps against alkaline degradation, or that it may also serve stabilize the CTD-arm and preserve its flexibility and binding propensity to subsequent RSV N protomers in non-optimal growth conditions.

Incubation of RSV N with short adenine-repeat RNA oligos results in helical filament formation

With low or high concentration of protein-RNA complex assembled with the Poly7A RNA construct and varying ionic strengths of the polymerization solution, higher-order oligomeric assemblies of N-RNA

were observed, labeled in yellow in the figure panels (Fig. 8). Additionally, relative to Figure 1A, using the same concentration of the poly7A construct in place of the longer Tr70 trailer RNA sequence resulted in a greater proportion of complete N-RNA ring assembly (Fig. 8A). Interestingly, doubling the ionic strength of solution by doubling the concentration of NaCl from 150 mM to 300 mM drastically reduces N-RNA ring formation propensity and efficiency when using the poly7A RNA construct compared to the Tr70 construct, suggesting that a greater oligo length can provide further stabilization favoring complete assembly and that using smaller RNA oligos may shift formation equilibrium towards a different direction. However, in comparing Fig. 5A and Fig. 8A, using a smaller RNA oligo length apparently shifts N-RNA formation tendency from incomplete oligomeric aggregation to helical filament formation, confirming previous results wherein the RSV N CTD arm is modeled as highly flexible and able to position itself within either the RNA-binding groove of the N_i protomer or to clasp via interaction onto the CTD of the consequent N_{i+1} nucleoprotein protomer [30]. This conformational flexibility of the nucleoprotein CTD-arm seems to be influenced to a great extent by a combination of RNA construct length and N-RNA complex concentration in solution.

The RSV N-RNA ring degrades when assembled in conditions of increasing alkalinity

In conditions of higher pH, there is significantly lower N-RNA ring formation efficiency with short RNA oligos, whereas propensity largely remains unaltered (Fig. 9). The increase in the proportion of incomplete NCLP assembly as the pH becomes more alkaline is reflective of the results drawn earlier: the higher pH implies lower proton concentration in solution and thus would result in a lower ionic strength when salt concentration is kept at 300 mM, an association also documented by previous literature in analyzing the formation of nanobubbles by colloidal, water-soluble organic particles in an aqueous suspension [31]. We then postulate that this decreases the flexibility of the CTD-arm due to the lower relative attenuation of the salt bridges which stabilize the linking interactions that pack the CTD-arm against the core of N, decreasing the likelihood of stable linking interactions forming with other

nucleoprotein protomers and of RNA binding to its respective groove within N. While we would expect N-RNA ring formation propensity to also decrease with increasing pH values for the reasons mentioned previously, the similarities in this regard between the panels may be due to the high affinity of RSV N-RNA particles for the support grid film and their subsequent preferred assembly and aggregation away from the central holes, making it difficult to accurately ascertain such differences.

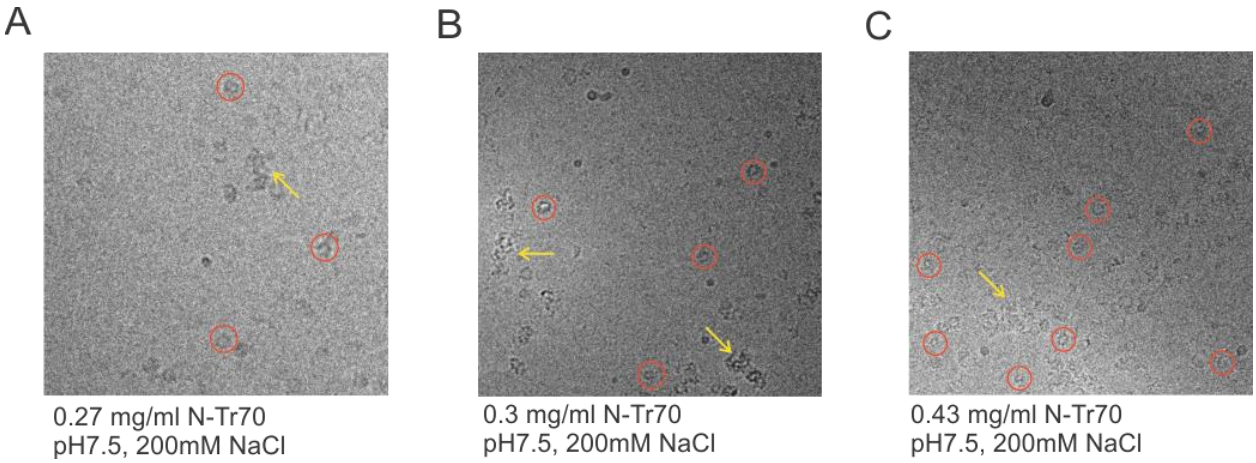

Figure 5: RSV NCLP assemblies consistently show aggregation in the absence of DTT. Yellow arrows denote regions of incomplete nucleocapsid-like particle (NCLP) aggregation and red circles specify instances of complete N-RNA ring assembly.

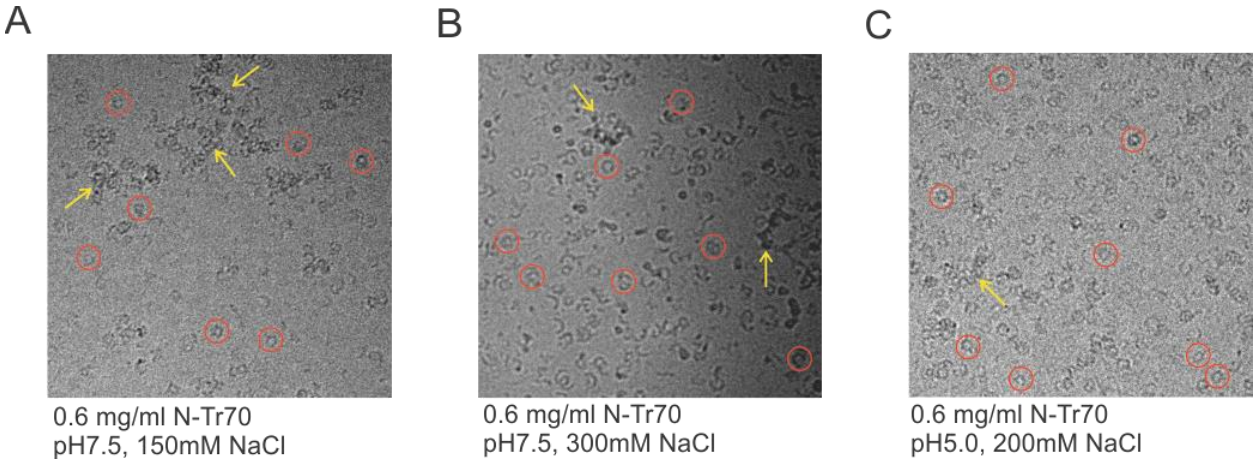

Figure 6: RSV NCLP propensity for assembly and construction efficiency are determined by solution pH and ionic strength. Yellow arrows denote regions of incomplete nucleocapsid-like particle (NCLP) aggregation and red circles specify instances of complete N-RNA ring assembly.

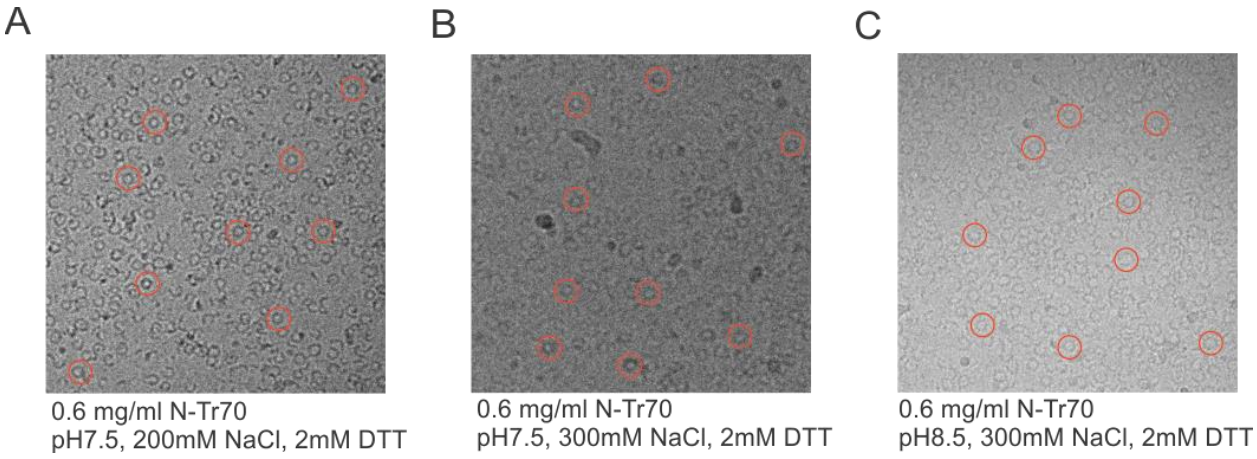

Figure 7: Presence of Dithiothreitol (DTT) maintains high efficiency and propensity of RSV NCLP assembly in alkaline pH conditions. Red circles specify instances of complete N-RNA ring assembly.

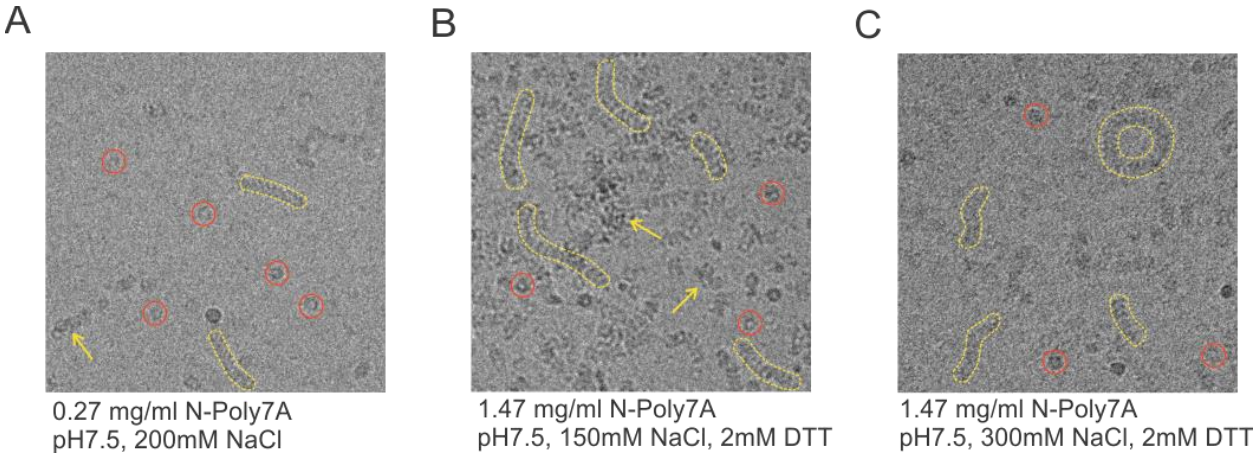

Figure 8: RSV NCLPs oligomerize into helical filaments when using short adenine repeats as RNA sequences. Yellow outlines denote helical filaments, yellow arrows denote regions of incomplete nucleocapsid-like particle (NCLP) aggregation, and red circles specify instances of complete N:RNA ring assembly. N:Poly7A assembles under different conditions (A) 0.27 mg/ml, pH7.5, 200mM NaCl; (B) 1.47 mg/ml, pH7.5, 150mM NaCl, 305 2mM DTT; (C) 1.47 mg/ml, pH7.5, 300mM NaCl, 2mM DTT.

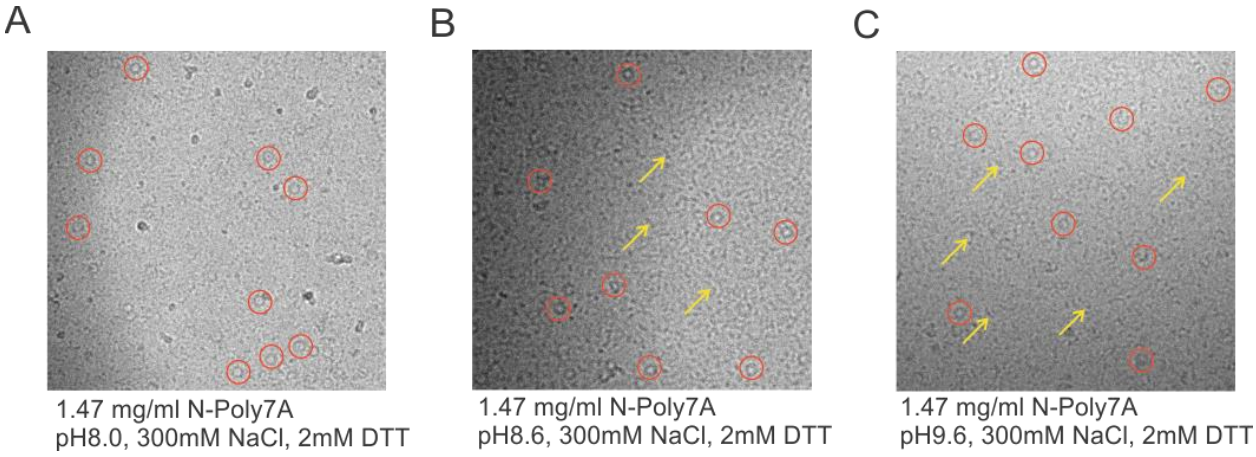

Figure 9: Significantly alkaline buffer conditions lead to degradation of the RSV NCLP assembly and increased aggregation of particles. Yellow arrows denote regions of incomplete nucleocapsid-like particle (NCLP) aggregation and red circles specify instances of complete N:RNA ring assembly. 1.47 mg/ml N:Poly7A assembles under different conditions (A) pH8.0, 300mM NaCl, 2mM DTT; (B) pH8.6, 300mM NaCl, 2mM DTT; (C) pH9.6, 300mM NaCl, 2mM DTT.

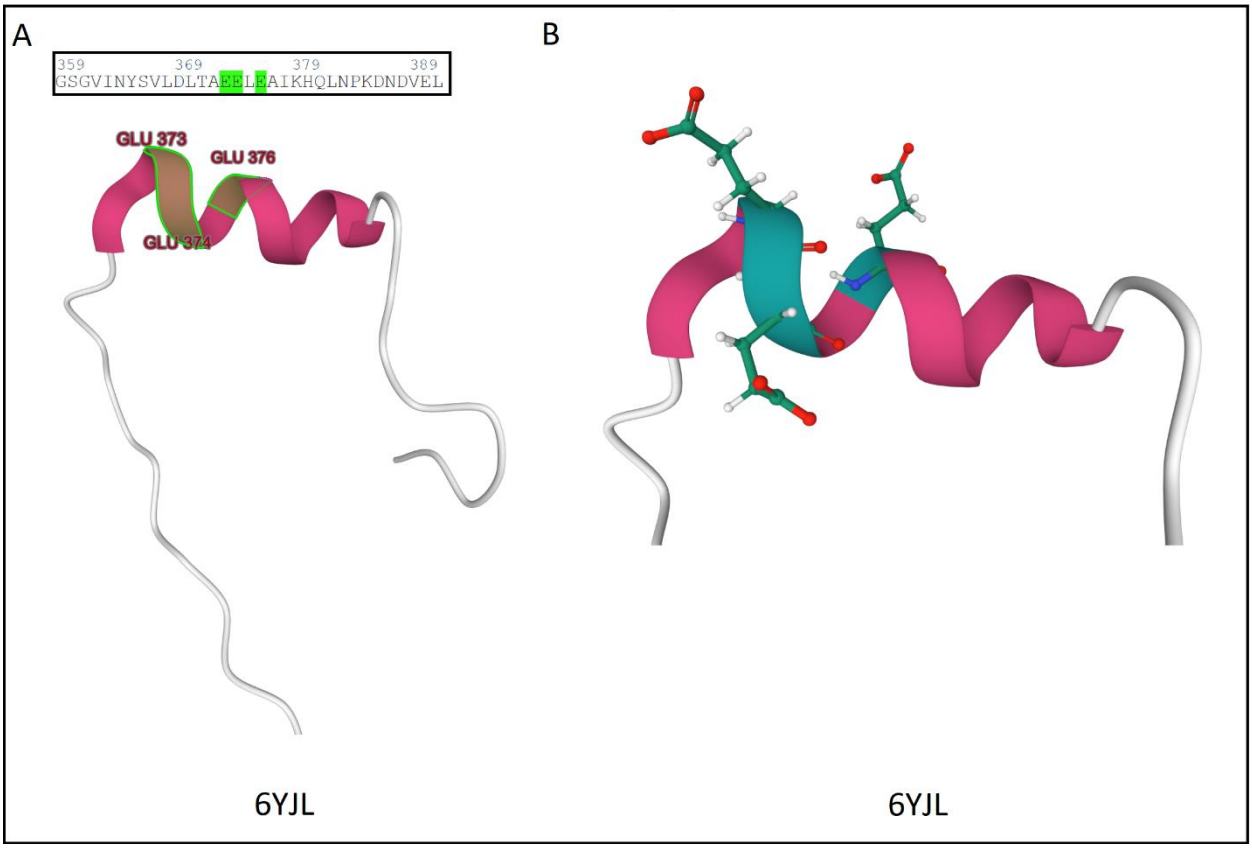

Figure 10: Solution NMR CTD-arm structure of RSV N. Image was created with the PyMOL plugin on the Protein Data Bank website with structure 6YJL [32]. (A) The pink region comprised of residues spanning 370 – 380 compose the helical segment, and the negatively charged residues within this segment are conserved throughout *Paramyxoviridae*. (B) A zoomed image consisting of ball-and-stick projections of the glutamic acid residues within the helical segment of the N CTD-arm.

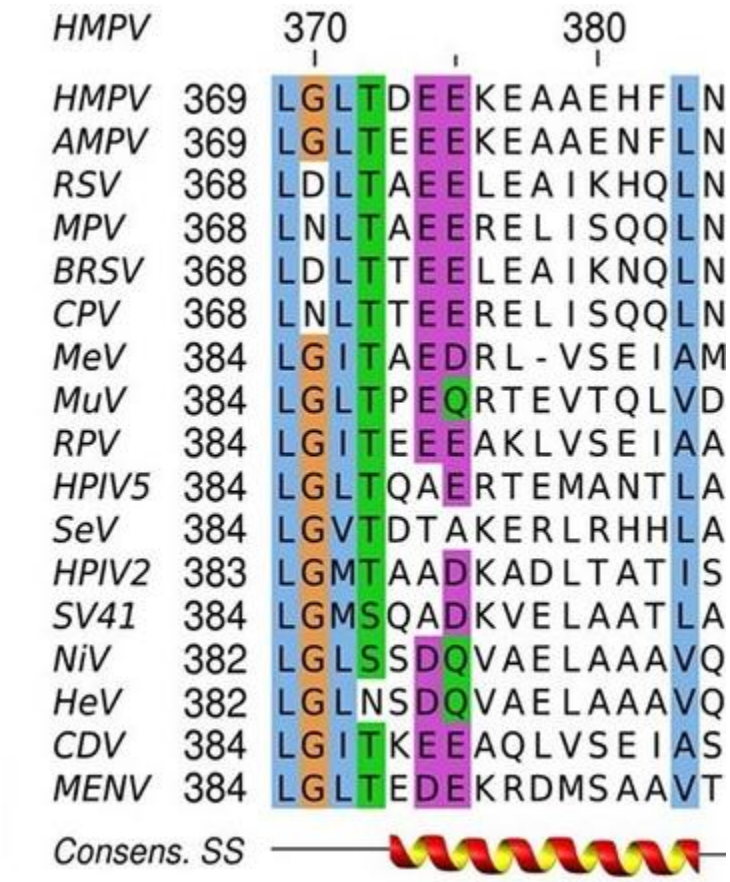

Figure 11: Nucleoprotein CTD-arm consensus sequences of Paramyxoviridae family members.

Negatively charged, acidic residues are highly conserved in the segment of the CTD arm with helical propensity (shown in purple). Other conserved residues are labeled in orange (glycine residues), teal (hydrophobic residues), green (hydrophilic uncharged residues). Figure adapted from Renner, M., et al. (2016) [16].

Discussion

Previous studies have characterized RSV P as an essential chaperone protein required for assembly of monomeric soluble N^0-P[18,33]. RSV P also functions in preventing both self-oligomerization of N^0 and non-specific binding to random cellular RNAs [22,34], and it has been previously delineated that the N-terminal domain of P is sufficient for maintaining the monomeric N^0 form [7,18]. Interestingly, it has also been noted in previous literature that in human RSV (hRSV), the CTD-arm of N is directly involved in inhibiting the associative interactions between N and RNA, and a general mechanism of RNA binding inhibition within the *Mononegavirales* order of viruses was postulated to involve a dual interaction between the N CTD-arm and the RNA binding domain as well as the binding of P_{NTD} to N such that interactions with other N protomers and non-viral specific RNAs are impaired [22]. Here, we postulate that P dissociation in order to activate monomeric N^0 occurs in tandem with the elevation of N CTD-arm flexibility to an optimal extent to configure the fully activated conformation of N^0 (Fig. 12), and we report that CTD-arm flexibility can be manipulated with alterations in solution ionic strength as well as with addition of DTT, with the latter apparently showing dependence on the RNA-length used for NCLP construction. In contrast to the rule of six observed in virus members of the *Paramyxoviridae* family where the requisite number of nucleotides in the viral genome must be a multiple of six [35,36], the rule does not hold for viruses of the *Pneumoviridae* family; the crystal structure of RSV N-RNA depicts that each N subunit contacts seven RNA nucleotides [11]. Thus, to judge RSV N-RNA formation propensity and efficiency with manipulations in RNA length we used shorter 7-nucleotide polyA oligos (poly7A) which we had previously established as sufficient in length for stimulating proper assembly of N–RNA [18]. In context of the perceived "rule-of-seven" and in keeping consistent with elucidating the associative propensity and efficiency of viral-specific RNAs, the longer RNA sequences consisted of 70 nucleotides from the 5' region of the RSV genomic RNA trailer sequence (Tr70).

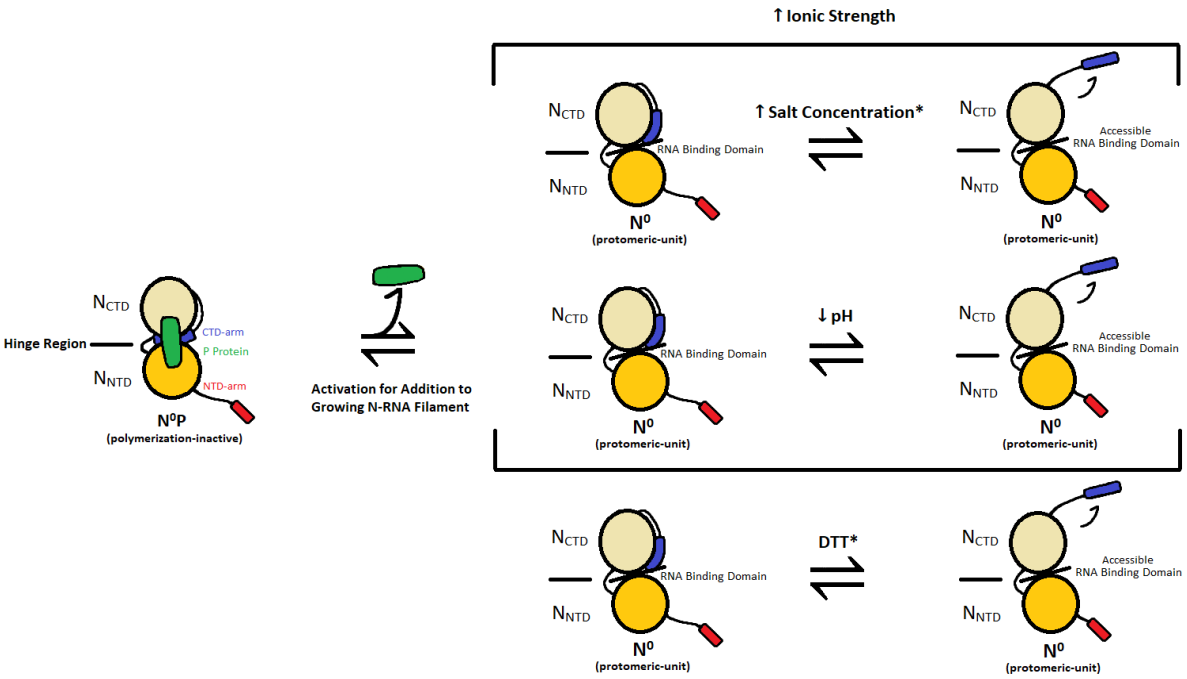

Figure 12: Figure depicting a model where release of the P peptide and proper CTD-arm orientation are essential for activation of N^0 for addition to the growing N-RNA filament, where the latter is influenced by (i) ionic strength and (ii) DTT* in an RNA-length dependent manner. The increase in ionic strength in solution was conferred either by an elevation in salt concentration or by reducing pH, both of which confer greater CTD-arm flexibility. DTT may preserve CTD-arm flexibility even when complexation occurs in higher pH or in other adverse conditions with lower ionic strengths, but the effect is solely observed for RSV N-RNA complexes constructed with the Tr70 RNA sequence. Conversely, DTT may also serve as a protectant for long-chain RNA sequences (not pictured here), allowing for optimal N-RNA assembly propensity and efficiency despite construction in lower ionic strengths.

As described in an earlier section, a high ionic strength confers destabilization of salt-bridging interactions that pack the CTD-arm against the core of the N-protomer, favoring placement of RNA nucleotides within the RNA-binding domain and subsequent CTD-arm linkage with the subsequent N protomer (which is dependent on the RNA sequence length) (Fig. 12). However, elevating ionic strength above an optimum value may lead to excessive CTD-arm flexibility to the extent that it may be entropically unfavorable to limit its flexibility despite any stabilizing interactions (Fig. 13). This stabilization may be conferred either by protomeric inactivation through association near the RNA binding groove of its resident N protomer (Fig. 13B), or polymerization via linkage to the consequent nucleoprotein protomer to form N-RNA oligomers. However, DTT may rescue N-RNA oligomerization in conditions of lower solution ionic strength, an effect observed when using Tr70 to construct N-RNA, by either preserving CTD-arm flexibility with insufficient ionic strength in solution or directly protecting RNA and promoting its interaction with the RNA-binding domain of RSV N or possibly even exert a combination of both. The mechanisms that result in these downstream effects, however, are at this point speculative and require further experimental characterization.

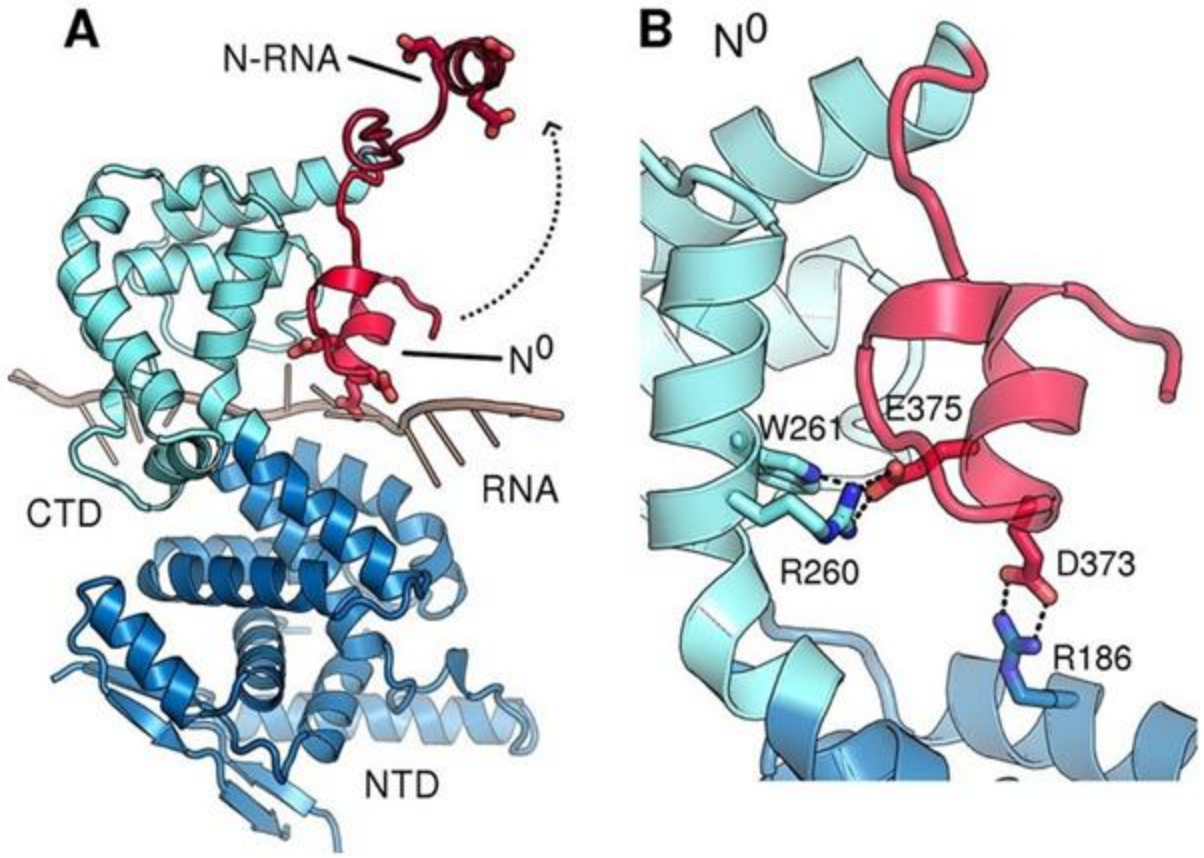

Figure 13: The N protein CTD arm prevents non-specific RNA interactions with N. The CTD-arm is shown in red, and the conformational switch is denoted with a dotted arrow. (A) The CTD-arm is in the upward conformation in the RNA-bound state but in the downward conformation in the RNA-free (N^0) state. (B) Specific salt bridging interactions (strong hydrogen bonding and ionic interactions) that restrict the CTD-arm (red) in the downward conformation. Figure adapted from Renner, M., et al. (2016) [16].

We thus propose three 10N-protomer assemblies: a left-handed ribonucleoprotein (RNP) helical oligomeric filament consistent with previous electron cryotomography elucidations [37], incompletely assembled N-RNA rings which are prone to aggregation, and rigid, complete assembly of 10-monomeric rings that do not display stacking into higher-order oligomeric structures (Fig. 14). Briefly, conformations 1 and 3 correspond to structures that are likely to assemble when using shorter RNA oligos & longer RNA sequences with optimal N CTD-arm flexibility respectively, but incomplete N-RNA ring formation, as shown in conformation 2, can result from excessive flexibility of the N CTD-arm, pictured when using longer RNA sequences. Further, aggregation occurs with excessive flexibility of the N CTD-arm regardless of RNA oligo length, which may be due to entropic unfavorability of limiting CTD-arm mobility by binding to the subsequent N protomer either above it, as is the case when utilizing poly7A RNA oligos, or to the next N protomer within the same plane, as is the case when utilizing Tr70 RNA oligos. Usage of shorter RNA oligos, here poly7A, seems to shift the function of the CTD-arm of RSV N to polymeric stabilization via packing when at optimal flexibility, building higher order helical filaments perhaps by binding to the N protomer positioned above it. With longer RNA sequences, here Tr70, the CTD-arm and NTD-arms of the protomeric N-unit latch onto neighboring protomers in an orchestrated fashion [13], wherein the NTD-arm of N_{i+1} binds to the flank of the N-terminal domain of N_i and the CTD-arm of N_{i-1} binds onto the C-terminal domain of N_i to make an energetically stable N-RNA rigid ring assembly (Fig. 14). These are speculations, and further quantitative studies are needed to understand partial N-RNA NCLP assembly. Additionally, further structural studies of *in vitro* assembled NCLPs characterizing CTD-arm orientation within a helical filament as opposed to within a rigid ring or within aggregates are required to justify the aforementioned proposals.

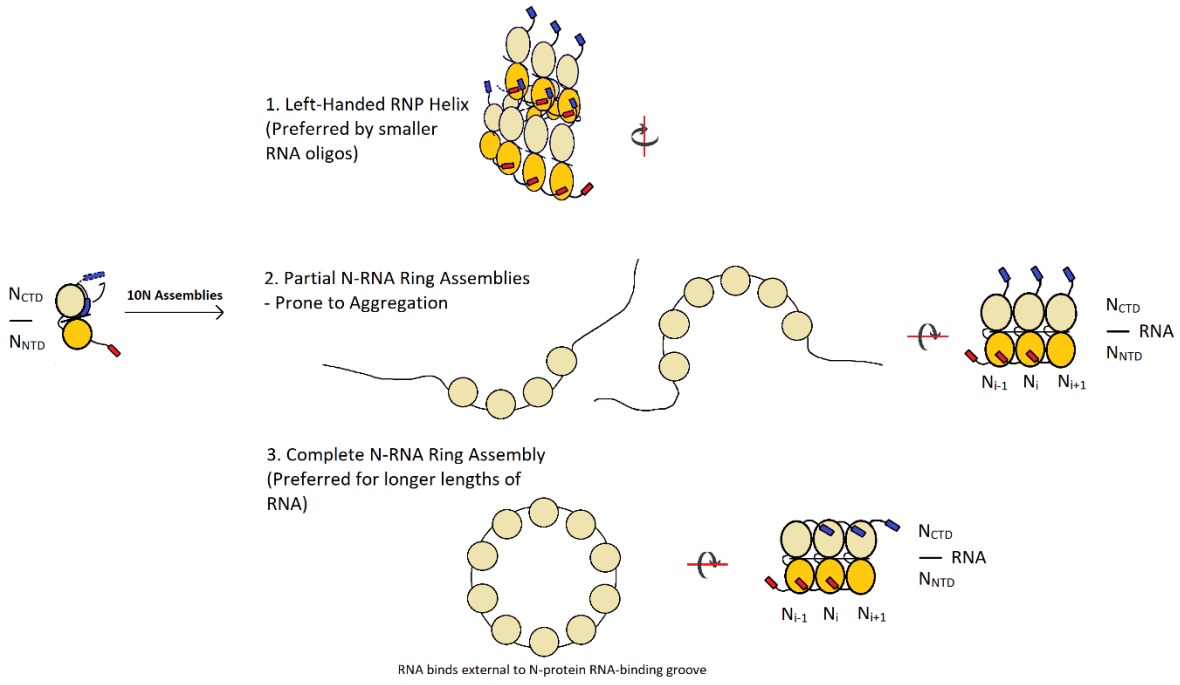

Figure 14: Figure depicting RSV decameric N-RNA assembly morphologies observed with manipulation of RNA length, ionic strength, and incorporation of DTT. The first structure is seen with N-RNA constructions utilizing poly7A and is left-handed in nature [37]. The second structure shows partial N-RNA rings as noted in N-RNA complexes with both RNA sequence lengths, but this morphology is notably more prominent in assemblies constructed with Tr70 RNA: rigid ring formation may be unfavorable due to the highly mobile CTD-arm though NTD association between protomers via NTD-arms may be still probable. When the CTD-arm is optimally flexible, in utilizing Tr70 the consequent N-RNA assemblies are rigid and stable with a predisposed association pattern between N_{i-1}, N_i, and N_{i+1}, as shown in the third structure. Corresponding PDB structures for the structures given in 1 and 3 are provided in Fig. S4.

Supplemental Figures

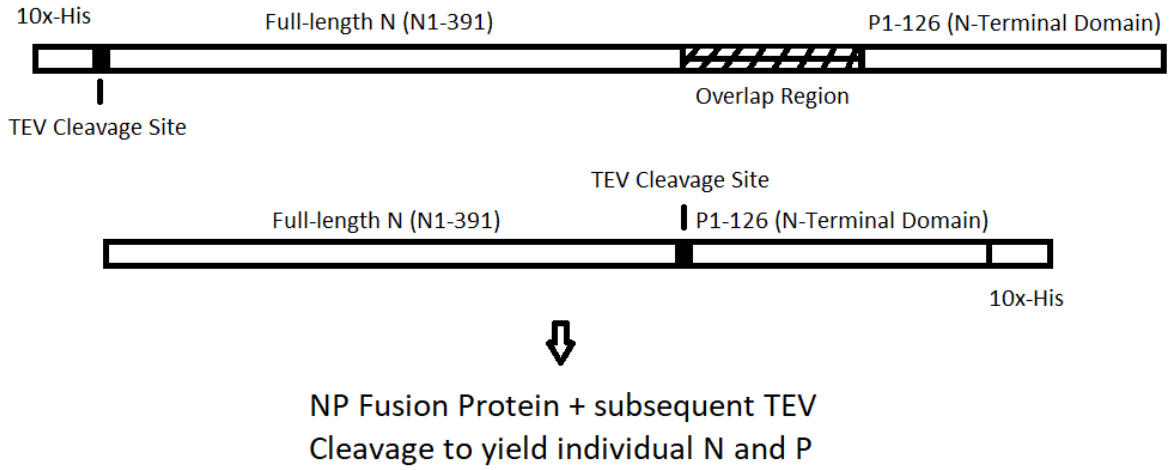

Figure S1: Schematic of the construct used for N_{FL}-P_{1-126}-10x-His production with high effiency.

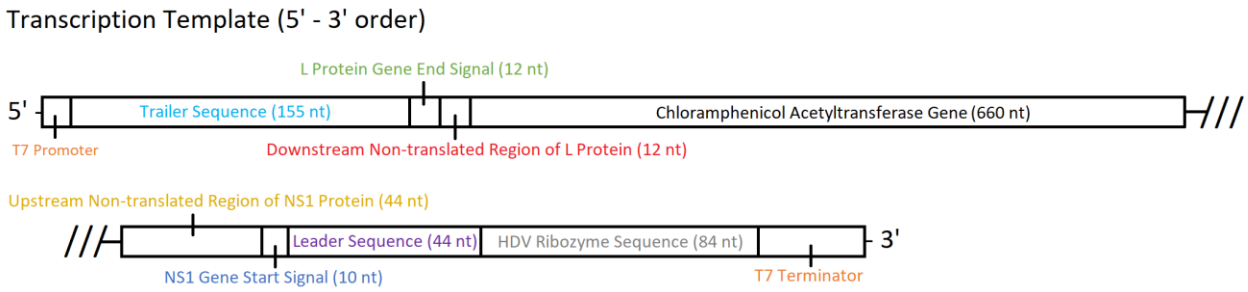

5'—
TAATACGACTCACTATAGGGACGAGAAAAAAAGTGTCAAAAACTAATATCTCGTAATTTAGTTAATACACATATAA
ACCAATTAGATTAGGGTTTAAATTTATTCCTCCAAGATTAAAATGATAACTTTAGGATTAGTTCACTAAAAGTTATTT
AAAAAATTATATGATTTTTAATTTTTAATAACTATAATTGAATACATGGAGAAAAAAGATCACCGGGTACACGACTGT
CGATATAAGTCAATGGCACCGAAAAGAGCATTTTGAGGCGTTCCAGTCCGTAGCGCAATGCACCTACAATCAGAA
GTCCAGCTGGATATCACGGCATTCCTCAAGACTGTCAAAAAAAATAAGCACAAGTTCTACCCGGCGTTTATCCATA
TACTCGCTAGACTCATGAACGCACACCCAGAATTTCGCATGGCAATGAAGGATGGGGAGCTTGTAATATGGGACT
CAGTTCATCCTTGTTATACAGTGTTTCACGAACAGACCGAGACTTTCAGTTCACTCTGGTCCGAATACCATGATGAT
TTCAGGCAATTCCTTCATATTTATTCACAGGATGTCGCTTGCTACGGGGAAAACCTTGCGTATTTCCCCAAAGGCTT
CATTGAAAACATGTTCTTCGTCAGTGCTAACCCTTGGGTTAGCTTTACATCTTTCGATTTGAACGTGGCAAATATGG
ACAATTTTTTTGCGCCCGTTTTTACTATGGGTAAATATTATACACAAGGGGATAAGGTGCTTATGCCGCTTGCAATC
CAAGTACACCATGCTGTGTGCGACGGATTTCATGTGGGGCGAATGCTTAACGAGCTGCAACAATACTGTGATGAA
TGGCAGGGGGGTGCTTAACTCTAACCAAGGGAGTTAAATTTAAGTGGTACTTATCAAATTCTTATTTGCCCCATTTT
TTTGGTTTATGCAAGTTTGTTGTACGCATTTTTTCGCGTTGAGTTACAGAGATGTAACTCTGTAACTCCTGATGAGT
CCGTGAGGACGAAACGAGAAAAAAAGTGTCAAAAACTAATATCTCGTAAAAAAACTAGCATAACCCCTTGGGGCC
TCTAAACGGGTCTTGAGGGGTTTTTTG
—3’

Figure S2: Diagram & color-coded sequence of the RSV chloramphenicol acetyltransferase (CAT) minigenome for *in vitro* transcription of RNA. The template consists of the T7 promoter (17 nt upstream of +1 transcription start site), L protein gene end (GE) signal (12 nt), the downstream non-translated region of L protein, the CAT gene (660 nt), the upstream non-translated region of NS1 (44 nt), the leader sequence (44 nt), and an 84 nt hepatitis delta virus (HDV) ribozyme sequence flanked at the 3’ end by poly7A sequence and the T7 terminator (48 nt).

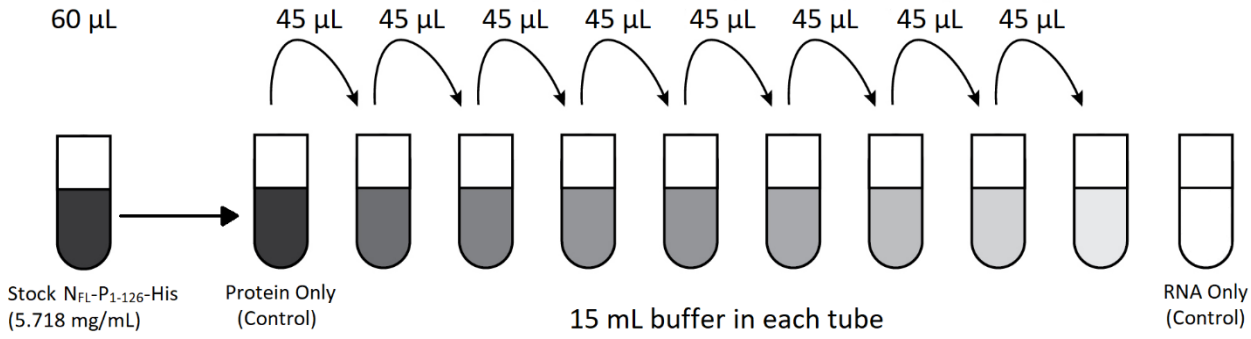

Figure S3: Schematic of serial dilution for Electrophoretic Mobility Shift Assay (EMSA).

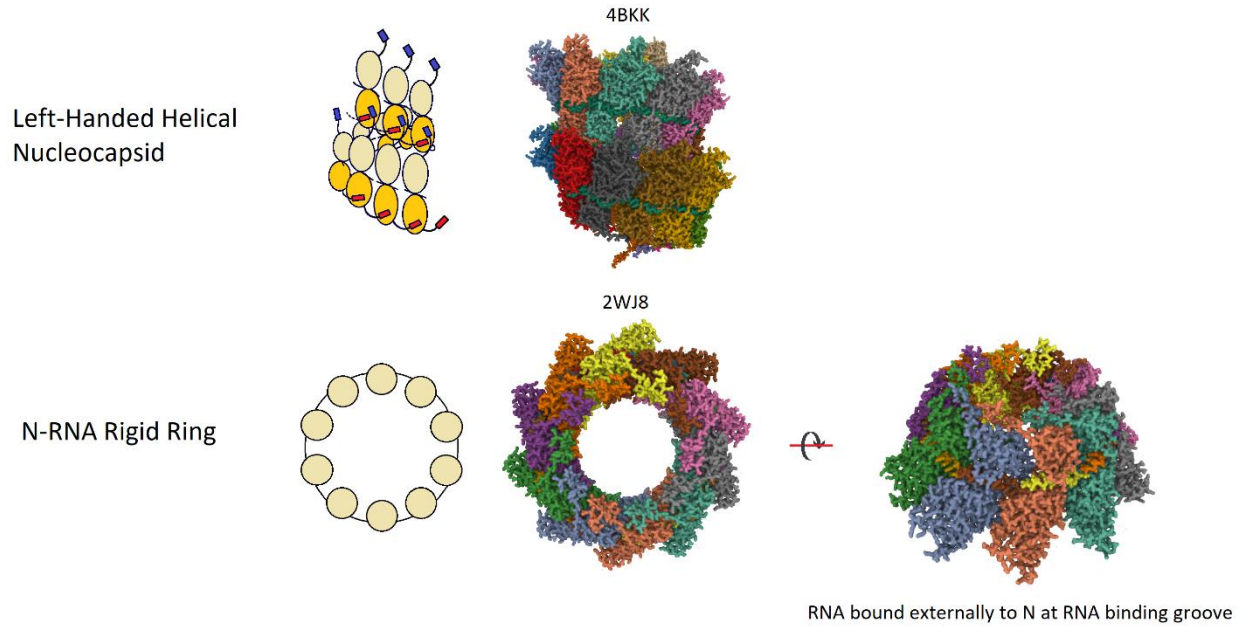

Figure S4: Protein Data Bank Images depicting N-RNA morphologies. Structures are Gaussian surface representations, generated with the PDB PyMOL plugin [38]. The PDB ID code for the RSV left-handed helical nucleocapsid is 4BKK, and the PDB ID code for the RSV N-RNA ribonucleoprotein ring is 2WJ8.

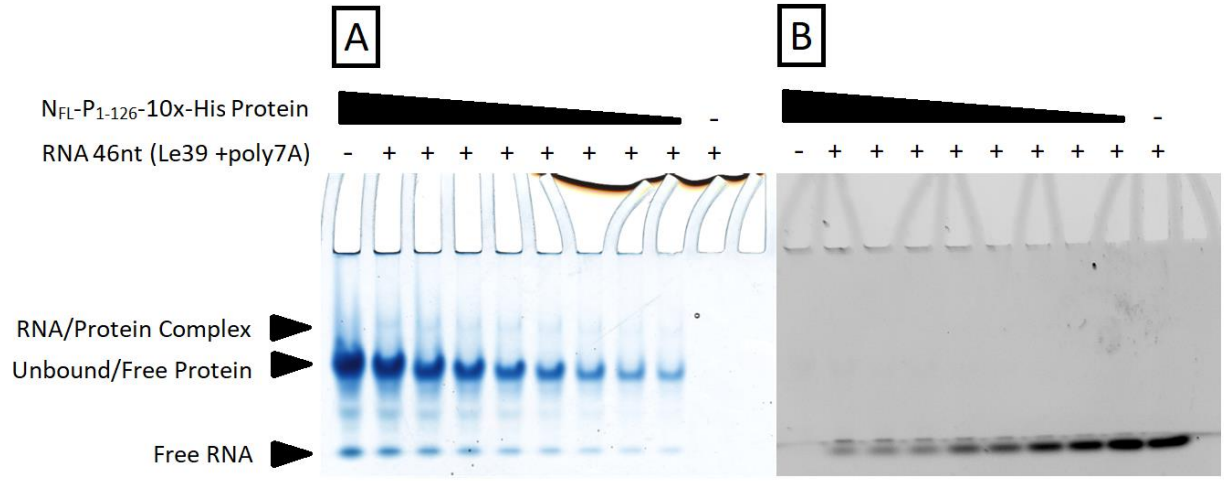

Figure S5: Electrophoretic Mobility Shift Assay (EMSA) depicts binding between N^0P and RNA.

(A & B) The 46 nucleotide RNA sequence comprised of the first 39 nucleotides of the leader sequence of the RSV CAT minigenome with a poly7A addendum was incubated with increasingly dilute concentrations of purified N_{FL}-P_{1-126}-10xHis overnight (lanes 2-8; dilution factor of 1.33). Lane 1 contains free protein only at stock concentration of 5.718 mg/mL and Lane 10 contains free RNA only at a concentration of 1 µM. Sample RNA concentration was uniform in lanes 2-10. (A) Image of Coomassie Blue stained gel. (B) Image of ethidium bromide stained and UV visualised gel.

References

1 Aggarwal, R. Lower airway disease caused by respiratory syncytial virus. *Indian J Pediatr* **65**, 355-362, doi:10.1007/bf02761127 (1998).

2 Piedimonte, G. & Perez, M. K. Respiratory syncytial virus infection and bronchiolitis. *Pediatr Rev* **35**, 519-530, doi:10.1542/pir.35-12-519 (2014).

3 Canedo-Marroquín, G. *et al.* Modulation of Host Immunity by Human Respiratory Syncytial Virus Virulence Factors: A Synergic Inhibition of Both Innate and Adaptive Immunity. *Front Cell Infect Microbiol* **7**, 367, doi:10.3389/fcimb.2017.00367 (2017).

4 Jafri, H. S. *et al.* Respiratory syncytial virus induces pneumonia, cytokine response, airway obstruction, and chronic inflammatory infiltrates associated with long-term airway hyperresponsiveness in mice. *J Infect Dis* **189**, 1856-1865, doi:10.1086/386372 (2004).

5 Bhella, D., Ralph, A., Murphy, L. B. & Yeo, R. P. Significant differences in nucleocapsid morphology within the Paramyxoviridae. *J Gen Virol* **83**, 1831-1839, doi:10.1099/0022-1317-83-8-1831 (2002).

6 Collins, P. L., Fearns, R. & Graham, B. S. Respiratory syncytial virus: virology, reverse genetics, and pathogenesis of disease. *Curr Top Microbiol Immunol* **372**, 3-38, doi:10.1007/978-3-642-38919-1_1 (2013).

7 Cao, D., Gao, Y. & Liang, B. Structural Insights into the Respiratory Syncytial Virus RNA Synthesis Complexes. *Viruses* **13**, 834 (2021).

8 Nam, H. H. & Ison, M. G. Respiratory syncytial virus infection in adults. *Bmj* **366**, l5021, doi:10.1136/bmj.l5021 (2019).

9 Cannon, M. J. Microplaque immunoperoxidase detection of infectious respiratory syncytial virus in the lungs of infected mice. *J Virol Methods* **16**, 293-301, doi:10.1016/0166-0934(87)90014-0 (1987).

10 Galloux, M. *et al.* Minimal Elements Required for the Formation of Respiratory Syncytial Virus Cytoplasmic Inclusion Bodies In Vivo and In Vitro. *mBio* **11**, e01202-01220, doi:doi:10.1128/mBio.01202-20 (2020).

11 Tawar, R. G. *et al.* Crystal Structure of a Nucleocapsid-Like Nucleoprotein-RNA Complex of Respiratory Syncytial Virus. *Science* **326**, 1279-1283, doi:10.1126/science.1177634 (2009).

12 Céspedes, P. F. *et al.* Surface expression of the hRSV nucleoprotein impairs immunological synapse formation with T cells. *Proc Natl Acad Sci U S A* **111**, E3214-3223, doi:10.1073/pnas.1400760111 (2014).

13 Galloux, M. *et al.* Identification and characterization of the binding site of the respiratory syncytial virus phosphoprotein to RNA-free nucleoprotein. *J Virol* **89**, 3484-3496, doi:10.1128/jvi.03666-14 (2015).

14 Tran, T. L. *et al.* The nine C-terminal amino acids of the respiratory syncytial virus protein P are necessary and sufficient for binding to ribonucleoprotein complexes in which six ribonucleotides are contacted per N protein protomer. *J Gen Virol* **88**, 196-206, doi:10.1099/vir.0.82282-0 (2007).

15 Castagné, N. *et al.* Biochemical characterization of the respiratory syncytial virus P-P and P-N protein complexes and localization of the P protein oligomerization domain. *J Gen Virol* **85**, 1643-1653, doi:10.1099/vir.0.79830-0 (2004).

16 Renner, M. *et al.* Nucleocapsid assembly in pneumoviruses is regulated by conformational switching of the N protein. *Elife* **5**, e12627, doi:10.7554/eLife.12627 (2016).

17 Bakker, S. E. *et al.* The respiratory syncytial virus nucleoprotein-RNA complex forms a left-handed helical nucleocapsid. *J Gen Virol* **94**, 1734-1738, doi:10.1099/vir.0.053025-0 (2013).

18 Gao, Y. *et al.* In vitro trackable assembly of RNA-specific nucleocapsids of the respiratory syncytial virus. *J Biol Chem* **295**, 883-895, doi:10.1074/jbc.RA119.011602 (2020).

19 Desfosses, A. *et al.* Self-organization of the vesicular stomatitis virus nucleocapsid into a bullet shape. *Nat Commun* **4**, 1429, doi:10.1038/ncomms2435 (2013).

20 Cao, D. *et al.* Cryo-EM structure of the respiratory syncytial virus RNA polymerase. *Nat Commun* **11**, 368, doi:10.1038/s41467-019-14246-3 (2020).

21 Kampjut, D., Steiner, J. & Sazanov, L. A. Cryo-EM grid optimization for membrane proteins. *iScience* **24**, 102139, doi:10.1016/j.isci.2021.102139 (2021).

22 Esneau, C. *et al.* Biochemical characterization of the respiratory syncytial virus N(0)-P complex in solution. *J Biol Chem* **294**, 3647-3660, doi:10.1074/jbc.RA118.006453 (2019).

23 Pylaeva, S., Brehm, M. & Sebastiani, D. Salt Bridge in Aqueous Solution: Strong Structural Motifs but Weak Enthalpic Effect. *Scientific Reports* **8**, 13626, doi:10.1038/s41598-018-31935-z (2018).

24 Harcourt, J. *et al.* Respiratory syncytial virus G protein and G protein CX3C motif adversely affect CX3CR1+ T cell responses. *J Immunol* **176**, 1600-1608, doi:10.4049/jimmunol.176.3.1600 (2006).

25 Hamza, A. *et al.* Structural Characterization and Binding Studies of the Ectodomain G Protein of Respiratory Syncytial Virus Reveal the Crucial Role of pH with Possible Implications in Host-Pathogen Interactions. *ACS Omega* **6**, 10403-10414, doi:10.1021/acsomega.1c00800 (2021).

26 Jeong, K. I. *et al.* CX3CR1 Is Expressed in Differentiated Human Ciliated Airway Cells and Co-Localizes with Respiratory Syncytial Virus on Cilia in a G Protein-Dependent Manner. *PLoS One* **10**, e0130517, doi:10.1371/journal.pone.0130517 (2015).

27 Chirkova, T. *et al.* CX3CR1 is an important surface molecule for respiratory syncytial virus infection in human airway epithelial cells. *J Gen Virol* **96**, 2543-2556, doi:10.1099/vir.0.000218 (2015).

28 Teng, M. N. & Collins, P. L. The Central Conserved Cystine Noose of the Attachment G Protein of Human Respiratory Syncytial Virus Is Not Required for Efficient Viral Infection In Vitro or In Vivo. *Journal of Virology* **76**, 6164-6171, doi:doi:10.1128/JVI.76.12.6164-6171.2002 (2002).

29 Battles, M. B. & McLellan, J. S. Respiratory syncytial virus entry and how to block it. *Nature Reviews Microbiology* **17**, 233-245, doi:10.1038/s41579-019-0149-x (2019).

30 Cox, R. & Plemper, R. K. The paramyxovirus polymerase complex as a target for next-generation anti-paramyxovirus therapeutics. *Frontiers in Microbiology* **6**, doi:10.3389/fmicb.2015.00459 (2015).

31 Jin, F., Li, J., Ye, X. & Wu, C. Effects of pH and Ionic Strength on the Stability of Nanobubbles in Aqueous Solutions of α-Cyclodextrin. *The Journal of Physical Chemistry B* **111**, 11745-11749, doi:10.1021/jp074260f (2007).

32 Cardone, C., Eleouet, J.-F.,Galloux, M.,Sizun, C. Solution NMR structure of the C-terminal arm of RSV nucleoprotein. doi:http://dx.doi.org/10.2210/pdb6yjl/pdb (To Be Published).

33 Jamin, M. & Yabukarski, F. in *Advances in Virus Research* Vol. 97 (eds Margaret Kielian, Thomas C. Mettenleiter, & Marilyn J. Roossinck) 143-185 (Academic Press, 2017).

34 Karlin, D. & Belshaw, R. Detecting remote sequence homology in disordered proteins: discovery of conserved motifs in the N-termini of Mononegavirales phosphoproteins. *PLoS One* **7**, e31719, doi:10.1371/journal.pone.0031719 (2012).

35 Calain, P. & Roux, L. The rule of six, a basic feature for efficient replication of Sendai virus defective interfering RNA. *J Virol* **67**, 4822-4830, doi:10.1128/jvi.67.8.4822-4830.1993 (1993).

36 Gutsche, I. *et al.* Structural virology. Near-atomic cryo-EM structure of the helical measles virus nucleocapsid. *Science* **348**, 704-707, doi:10.1126/science.aaa5137 (2015).

37 Liljeroos, L., Krzyzaniak, M. A., Helenius, A. & Butcher, S. J. Architecture of respiratory syncytial virus revealed by electron cryotomography. *Proc Natl Acad Sci U S A* **110**, 11133-11138, doi:10.1073/pnas.1309070110 (2013).

38 Sehnal, D. *et al.* Mol* Viewer: modern web app for 3D visualization and analysis of large biomolecular structures. *Nucleic Acids Res* **49**, W431-w437, doi:10.1093/nar/gkab314 (2021).